

UC Riverside

UC Riverside Previously Published Works

Title

^{13}C and $^{63,65}\text{Cu}$ ENDOR studies of CO Dehydrogenase from *Oligotropha carboxidovorans*.
Experimental Evidence in Support of a Copper-Carbonyl Intermediate

Permalink

<https://escholarship.org/uc/item/7xd9k84p>

Journal

Journal of the American Chemical Society, 135(47)

ISSN

0002-7863

Authors

Shanmugam, Muralidharan
Wilcoxon, Jarett
Habel-Rodriguez, Diana
[et al.](#)

Publication Date

2013-11-27

DOI

10.1021/ja406136f

Peer reviewed



Published in final edited form as:

J Am Chem Soc. 2013 November 27; 135(47): 17775–17782. doi:10.1021/ja406136f.

¹³C and ^{63,65}Cu ENDOR studies of CO dehydrogenase from *Oligotropha carboxidovorans*. Experimental evidence in support of a copper-carbonyl intermediate

Muralidharan Shanmugam¹, Jarett Wilcoxon², Diana Habel-Rodriguez³, George E. Cutsail III¹, Martin L. Kirk^{3,*}, Brian M. Hoffman^{1,*}, and Russ Hille^{2,*}

¹Department of Chemistry, Northwestern University, Evanston, IL 60208-3113

²Department of Biochemistry, University of California, Riverside, CA 92521

³Department of Chemistry, The University of New Mexico, Albuquerque, NM 87131-0001

Abstract

We report here an ENDOR study of an $S = 1/2$ intermediate state trapped during reduction of the binuclear Mo/Cu enzyme CO dehydrogenase by CO. ENDOR spectra of this state confirm that the ^{63,65}Cu exhibits strong and almost entirely isotropic coupling, show that this coupling atypically has a positive sign, $a_{\text{iso}} = +148$ MHz, and indicate an apparently undetectably small quadrupolar coupling. When the intermediate is generated using ¹³CO, coupling to the ¹³C is observed, with $a_{\text{iso}} = +17.3$ MHz. A comparison with the couplings seen in related, structurally assigned Mo(V) species from xanthine oxidase, in conjunction with complementary computational studies, leads us to conclude that the intermediate contains a partially reduced, Mo(V)/Cu(I), center with CO bound at the copper. Our results provide strong experimental support for a reaction mechanism that proceeds from a comparable complex of CO with fully oxidized, Mo(VI)/Cu(I), enzyme.

Keywords

CO dehydrogenase; Molybdenum binuclear center; ENDOR spectroscopy

Introduction

Carbon monoxide dehydrogenase from *Oligotropha carboxidovorans*¹ is a member of the xanthine oxidase family of molybdenum-containing enzymes^{2,3} that catalyzes the oxidation of CO to CO₂ (Scheme 1), transferring the reducing equivalents thus obtained into the quinone pool of the organism⁴. The reaction is essential for the organism when growing on CO as the sole source of both carbon and energy.

*Corresponding Author: To whom reprint requests should be directed at russ.hille@ucr.edu.

Supporting material Figure S1: 9.5 GHz EPR spectra of the CO dehydrogenase binuclear signal reduced with ^{12,13}CO. Figure S2: 2-D ¹³C-Davies ENDOR spectra of the binuclear center of CO dehydrogenase collected at selected magnetic fields across the EPR envelope, 2 K. This material is available free of charge via the Internet at <http://pubs.acs.org>

The enzyme has been characterized crystallographically^{5,6}, and found to be an $(\alpha\beta\gamma)_2$ heterohexamer, with a pair of [2Fe-2S] clusters in its small subunits (CoxS, 17.8 kDa), FAD in its medium subunits (CoxM, 30.2 kDa), and a unique binuclear Mo(VI)/Cu(I) cluster in the large subunits (CoxL, 88.7 kDa) of oxidized enzyme. The binuclear cluster is the site at which CO is oxidized and has the structure shown in Figure 1, with the two transition metals linked by a μ -sulfido bridge⁶. In the course of reduction of the enzyme by excess CO, the binuclear cluster exhibits a Mo(V) EPR signal with $\mathbf{g} = [2.0010, 1.9604, 1.9549]$ and large hyperfine coupling to the $I = 3/2$ $^{63,65}\text{Cu}$ nuclei, $\mathbf{A}(^{63,65}\text{Cu}) = [117, 164, 132]$ MHz⁷. The signal exhibits no proton super-hyperfine structure and is unchanged when the sample is prepared in D_2O , but modest line-broadening is observed when ^{13}CO is used as substrate suggesting coupling to the carbon atom derived from substrate⁷.

Both the μ -sulfido ligand and the Cu(I) ion of the binuclear cluster can be removed by treating the enzyme with cyanide, and a reconstitution protocol has been developed using Cu(I)•thiourea as the copper source. Alternatively, when Ag(I)•thiourea is used the Ag(I) ion is reconstituted into the active site. The Ag(I) substituted enzyme remains active and is reduced by CO with a limiting rate constant of 8.2 s^{-1} , as compared with 51 s^{-1} for the native Cu-containing form of the enzyme⁸. In the course of reduction by CO, the Ag(I) substituted form of the enzyme also exhibits a characteristic EPR signal, with $\mathbf{g} = [2.0043, 1.9595, 1.9540]$ and with strong coupling to the $I = 1/2$ $^{107,109}\text{Ag}$ nuclei with $\mathbf{A}(^{107,109}\text{Ag}) = [82, 79, 82]$ MHz.

Several structures can be envisaged for the EPR-active Mo(V) form of the native copper-containing CO dehydrogenase, as illustrated in Figure 2. Structure A is the Mo(V)-containing analog of a proposed Mo(IV)-containing intermediate in the reaction of enzyme with CO based on the 1.1-Å resolution structure of the enzyme in complex with *n*-butylisocyanide, in which the inhibitor is found to insert between the S-Cu bond of the μ -sulfido bridge (Figure 2, Structure A').⁶ The Mo(V) species would be formed from an initial Mo(IV) species by transfer of one electron from the binuclear cluster to the other redox-active centers of the enzyme prior to completion of the reaction (in a manner analogous to generation of the "very rapid" Mo(V) species seen with xanthine oxidase^{9,10,11}). Structure B represents an alternate reaction intermediate proposed on the basis of density functional studies of the binuclear center,^{12,13} with the Mo(V) species again generated by one-electron oxidation of a Mo(IV) species. Structure C is a Mo(V)-containing analog of the presumed complex of CO with oxidized enzyme that is believed to represent the initial intermediate in catalysis. Here, the CO is coordinated to the Cu(I) with a residual electron remaining in the binuclear center after reaction with a prior equivalent of CO (in this case, partial reduction of the center would have occurred by reaction of a prior equivalent of CO). In all three structures, the molybdenum is formally Mo(V) and the copper is Cu(I).

To discriminate among these structural alternatives and gain insight into the mechanism of CO oxidation, we have used 35 GHz pulsed-ENDOR spectroscopy to determine the ^{13}C , $^{95,97}\text{Mo}$, and $^{63,65}\text{Cu}$ hyperfine coupling tensors and the $^{63,65}\text{Cu}$ quadrupole coupling interaction for $^{12,13}\text{CO}$ -reduced CO dehydrogenase. The measured ^{13}C -hyperfine coupling is compared with reported ^{13}C -coupling for paramagnetic Mo(V) species observed with other members of the xanthine oxidase family, and the magnitude and sign of

the $^{63,65}\text{Cu}$ couplings are compared with those of other Cu centers. The combination of these measurements with DFT calculations discriminates among the potential structures for the intermediate (Figure 2), and support a spin-delocalized $[\text{Mo(V)}-(\mu\text{-S})\text{-Cu(I)}]$ structure that has CO coordinated to Cu(I). This species represents a paramagnetic analog of the initial $[\text{Mo(VI)}-(\mu\text{-S})\text{-Cu(I)}\cdot\text{CO}]$ Michaelis complex of the catalytic cycle, from which a catalytic sequence can be developed.

Materials and Methods

Carbon monoxide gas was obtained from Air, Inc. at a purity of 99.5 % and ^{13}C at 99 % enrichment was from Cambridge Isotope Laboratories. All other reagents were obtained at the highest level of purity available commercially. *O. carboxidovorans* (ATCC 49405) cells were grown at 30°C, pH 7.0 in a 20 L fermentor (BioFlo 415, New Brunswick) containing minimal medium and CO as the carbon source (introduced as a mixture of 50 % CO and 50 % air). Cells were harvested in late log phase ($\text{OD}_{436} > 5$), washed in 50 mM HEPES (pH 7.2) and stored at -80°C until needed. CO dehydrogenase was purified according to the procedure described by Zhang *et al.*⁷, using a combination of Q-Sepharose and Sephacryl S-300 FPLC chromatography. Enzyme was routinely reconstituted with copper using the method of Resch *et al.*¹⁴, and the degree of functionality determined by comparing the extent of enzyme bleaching, as observed at 450 nm, by CO (which reduces only the fully functional enzyme) with that seen using dithionite (which reduces both functional and nonfunctional enzyme); this typically exceeded 50 %.

ENDOR samples were prepared by making the enzyme (at a concentration of $\sim 200\ \mu\text{M}$) anaerobic by cyclic evacuation and flushing with O_2 -scrubbed argon gas for 1 h, followed by reduction under 1 atmosphere of CO for 30 s prior to freezing in a dry ice-acetone bath and storage in liquid N_2 . Accumulation of the EPR-active state was confirmed by EPR, using a Bruker Instruments ER 300 spectrometer equipped with an ER 035M gaussmeter and HP 5352B microwave frequency counter. Temperature was controlled at 150 K using a Bruker ER 4111VT liquid N_2 cryostat. 35 GHz pulsed EPR/ENDOR spectra were recorded as reported previously.^{15,16}

Spin-unrestricted gas-phase geometry optimizations for all CO dehydrogenase structures were performed at the density functional level of theory (DFT) using the ORCA software package (an *ab initio*, DFT and semiempirical SCF-MO package, version 2.8-20, September, 2010). All calculations employed the B3LYP hybrid exchange-correlation functional and a TZVP basis set for all atoms. DFT bonding calculations and EPR calculations used a scalar relativistic Hamiltonian, and the radial integration accuracies for Mo and Cu were increased as recommended for heavy atoms. The enzyme active site was represented by a Mo(V) ion with an apical oxo ligand and an equatorial ene-1,2-dithiolate ligand, either an equatorial oxo or hydroxy ligand, and an equatorial μ -sulfido ligand bridged to Cu(I)-SCH₃. EPR spin-Hamiltonian parameters were calculated for these two structures and various postulated CO/HCO₃-bound Mo(V) forms. Geometry optimizations were performed without constraints as well as with select bond and dihedral angles in the $\text{O}_{\text{apical}}\text{-Mo-S-Cu-S}$ chain constrained to maintain geometries consistent with those seen in the enzyme crystal structure.

Results

X-band (~ 9.5 GHz) EPR spectra of CO-reduced CO dehydrogenase were collected for samples prepared with $^{12,13}\text{CO}$ in H_2O 50 mM HEPES buffer, pH 7.2 at 150 K (Figures 3 (top) and S1). The EPR spectrum of the binuclear center of the enzyme generated with ^{12}CO (black line) shows a well-resolved structure centered around $g \sim 1.96$ with complex multiplet features due to hyperfine interactions with both Mo [$I(^{95,97}\text{Mo}) = 5/2$; 25 % natural abundance] and Cu [$I(^{63,65}\text{Cu}) = 3/2$; 100 % natural abundance] nuclei. In addition to the [Mo, Cu] cluster, the enzyme contains two [2Fe-2S] centers. However, at liquid nitrogen temperatures and above, the EPR signals arising from the iron-sulfur centers relax very fast and are not detected,

The 150 K X-band spectrum of the [Mo, Cu] center is well reproduced (red dashed line) with the following spin-Hamiltonian parameters: \mathbf{g} is roughly axial, $\mathbf{g} = [2.002, 1.958, 1.953]$; $\mathbf{A}(^{63,65}\text{Cu})$ is dominated by the isotropic interaction, $|\mathbf{A}(^{63,65}\text{Cu})| = [117, 164, 132]$ MHz, corresponding to $|a_{\text{iso}}(^{63,65}\text{Cu})| = 138$ MHz, with a small anisotropic coupling, $\mathbf{T} = [-21, 26, -7]$, having a maximum anisotropic component, $|T_{\text{max}}(^{63,65}\text{Cu})| = 26$ MHz.⁷ The g values, all being g_e , indicate that the EPR signal arises from a Mo(V) rather than Cu(II) species. A 2K echo-detected Q-band EPR spectrum of the same sample, Figure 3, lower, clearly shows the features of the [Mo, Cu] center, as can be seen by comparison with a simulation computed using $^{63,65}\text{Cu}$ hyperfine parameters determined by ENDOR, below. At this temperature, however, the EPR signals from the [2Fe-2S] centers relax slowly and overlap that of the binuclear center and their features are much more prominent owing to the greater degree of reduction of the iron-sulfur centers (40–50%) as compared to the fraction of the binuclear center that is paramagnetic (no greater than 15%). The spectrum gives no evidence for magnetic coupling between the binuclear center and the proximal [2Fe-2S] cluster, as expected given the conditions the sample was prepared (ie. by partial reduction of the substrate).

A preliminary set of X-band and Q-band spectra collected between 150 K and 77K confirm the above g -tensor, but shows that the small hyperfine anisotropy seen at 150K decreases upon cooling; this finding is extended in 2K ENDOR measurements presented below.¹ When the binuclear signal is generated using ^{13}CO , the X-band spectrum shows significant line broadening (Figure S1) due to unresolved hyperfine coupling to the ^{13}C , as previously reported.¹⁴

The g values for the EPR signal of the binuclear center, all being g_e , indicate that the signal arises from a Mo(V) rather than Cu(II) species, consistent with the known constitution of the binuclear center, with Mo(VI) and Cu(I) in the fully oxidized state. This conclusion is supported by contrasting the nearly isotropic $^{63,65}\text{Cu}$ hyperfine tensor with the highly anisotropic hyperfine coupling observed for Cu(II) systems.¹⁷ The conclusion is confirmed below by ENDOR measurements that determine the signs of the $^{63,65}\text{Cu}$ couplings.

¹This temperature dependence is not central to the present paper and will be described in detail elsewhere.

The overlap at 2K of the EPR signals from the slowly-relaxing [2Fe-2S] centers causes no problem for ENDOR measurements of the [Mo, Cu] binuclear center, as the ^{13}C and $^{63,65}\text{Cu}$ nuclei being studied by ENDOR are associated only with the [Mo, Cu] center. ^{13}CO signals are identified by comparing centers prepared with $^{12,13}\text{CO}$, and the [2Fe-2S] centers give no ENDOR response in the vicinity of $^{63,65}\text{Cu}$ ENDOR transitions.^{20–23}

Davies ENDOR spectra of the binuclear center of CO dehydrogenase, recorded at 2 K and taken at $g = 1.971$, are shown in Figure 4 (*top*) for samples reduced by $^{12,13}\text{CO}$. The $\nu^+ = 23$ MHz branch of the ^{13}C doublet ($\nu^\pm(^{13}\text{C}) = |A(^{13}\text{C})/2 \pm \nu(^{13}\text{C})|$) from ^{13}CO is evident in the latter case.² At the field of observation, $\nu(^{13}\text{C})$ is ~ 13.5 MHz, yielding $A(^{13}\text{C}) \sim 19$ MHz for the ^{13}C -hyperfine coupling. The ENDOR intensity in the 9–16 MHz region for both labeled and unlabeled samples can be assigned to amide ^{14}N features from the two [2Fe-2S] clusters, whose EPR signals overlap the Mo(V) EPR signal at low temperature (Figure 3; bottom). Subtraction of the ^{12}CO background (black line) from the ^{13}CO spectrum (red line) of the binuclear cluster more clearly shows the ν^+ peak (red dotted line), but also reveals the ν^- branch of the ^{13}C -doublet (relaxation effects lead to the reduced intensity for ν^-). Figure 4 (*bottom*) shows a 2-D field-frequency plot of the background-subtracted Davies ^{13}C -ENDOR spectra for the binuclear cluster of CO dehydrogenase reduced by ^{13}CO , recorded at selected magnetic fields across the EPR envelope (For complete 2-field-frequency pattern, see Figure S2). The frequencies of the ^{13}C doublet remain essentially constant over the entire absorption envelope, and the pattern can be simulated by the hyperfine tensor, $\mathbf{A}(^{13}\text{C}) = +[16.7, 16.5, 18.8]$ MHz. The ^{13}C hyperfine tensor is thus dominated by an isotropic coupling of $a_{\text{iso}}(^{13}\text{C}) = +17.33$ MHz, with an extremely small anisotropic term that approximates the dipolar form: $\mathbf{T} = [-T, -T, 2T]$ where $T = 0.73$ MHz. These results are summarized in Table 1.

Figure 5 shows a 2-D field-frequency plot of Davies ENDOR spectra collected over the frequency range of 30–100 MHz at multiple field settings across the EPR envelope for the spectrum seen with enzyme reduced by ^{12}CO . At all magnetic field settings the spectra exhibit a strong ^1H -ENDOR response arising from weakly coupled proton(s) without well-resolved structure. These ^1H -ENDOR features overlap with ENDOR features attributable to $^{95,97}\text{Mo}$ ($I = 5/2$), isotopes that together account for 25 % of the total isotopic abundance. These features are similar to those that have been seen previously in the ENDOR spectrum of the formaldehyde-inhibited Mo(V) signal of xanthine oxidase²⁴. Because of the poor resolution and low natural abundance, combined with the additional complexity arising from strong quadrupolar coupling in the case of ^{97}Mo , no attempt has been made to simulate this pattern. However, its overall character indicates that the isotropic hyperfine coupling for molybdenum, $a_{\text{iso}}(^{95,97}\text{Mo})$, is roughly 75–125 MHz.²⁵

The hyperfine tensor measured in the X-band EPR spectrum from the overlapping splittings of ^{63}Cu (69 %), and ^{65}Cu (30 %), predicts the presence of a Q-band $^{63,65}\text{Cu}$ ENDOR response from the $\nu^+(^{63,65}\text{Cu})$ manifold in the frequency range, ~ 75 –100 MHz. The Q-band ENDOR spectra taken at 2 K exhibit the predicted response, with $\nu^+(^{63,65}\text{Cu}) \sim 90$ MHz (Figure 5, blue horizontal bar) corresponding to a hyperfine coupling of $|A(^{63,65}\text{Cu})| = 148$

²Assignment as ν^- would yield a hyperfine coupling too large to be compatible with the X-band EPR spectra.

MHz, within the range of values expected from the EPR-derived hyperfine tensor. The signals are exceedingly sharp compared to those seen for a Cu(II) protein²⁶; and there is no evidence in the ENDOR spectra for the significant quadrupolar coupling to the $I = 3/2$ nuclear spin of $^{63,65}\text{Cu}$ seen in Cu(II) proteins.

The frequency of this $^{63,65}\text{Cu}$ signal remains constant as the field is moved towards g_2 and g_3 , indicating that the hyperfine interaction is isotropic within experimental error, with $a_{\text{iso}}(^{63,65}\text{Cu}) = +148$ MHz, a slight increase from, $a_{\text{iso}}(^{63,65}\text{Cu})$ obtained from the continuous-wave EPR spectra at higher temperature, Table 2. The vanishing of the anisotropic coupling upon cooling to 2K is compatible with the temperature variation of the small $^{63,65}\text{Cu}$ hyperfine anisotropy seen at higher temperatures (see above). This phenomenon may be assigned to changes in the geometry at Cu(I) with cooling. It is well known that considerable changes in the geometry of a diatomic bound to a metal ion can occur during cooling,²⁷ and this quite likely is happening to the Cu-CO linkage. However, the spectra collected towards the high field/low- g -value edge of the EPR spectrum do show a ‘tailing’ towards higher frequency that may reflect a heterogeneity in the geometry at Cu(I). For consistency, the 2K ENDOR-derived $^{63,65}\text{Cu}$ coupling will be used in the following discussion.

Signs for the hyperfine tensors, which are not available from EPR measurements, were determined from the ENDOR spectra of the binuclear cluster (more specifically, the sign of $g_{\text{Nuc}}A_{\text{Nuc}}$) using the Pulse-Endor-Saturation-Recovery (PESTRE) protocol, a pulse sequence comprised of multiple Davies ENDOR sequences^{28,29}. Figure 6 shows the PESTRE measurements obtained at $g = 1.975$ for the ν^+ branches of the ^{13}C and $^{63,65}\text{Cu}$ -ENDOR responses, where relatively sharp ENDOR responses for ^{13}C and $^{63,65}\text{Cu}$ nuclei are observed. In phase I of the PESTRE traces (no radio frequency illumination), the ν^+ branches of the ^{13}C and $^{63,65}\text{Cu}$ have reached the steady-state electron spin-echo baseline; in phase II, radio frequency excitation is applied and converts the spin populations and spin-echo response to their steady-state ENDOR values; in phase III (again in the absence of radio frequency illumination), the electron-nuclear spin populations give rise to a spin-echo signal denoted as the dynamic reference level, which relaxes to the BSL. In phase III, the ν^+ signals of ^{13}C (red line) and ^{63}Cu (blue line; inset) both relax to the spin-echo baseline ‘from below’, behavior that unambiguously establishes that both $A(^{13}\text{C})$ and $A(^{63,65}\text{Cu})$ are positive.

Discussion

The aim of the present investigation is to determine the structure of the species that gives rise to the EPR signal seen upon partial reduction of CO dehydrogenase with CO, and to use this information in conjunction with DFT calculations to elucidate the reaction mechanism of the enzyme. The experimental and computational results are summarized in Table 2, where it can be seen that the most remarkable feature of this species is the large and positive *isotropic* hyperfine coupling to copper, with $a_{\text{iso}}(^{63,65}\text{Cu}) = +148$ MHz, with negligible anisotropic hyperfine coupling to the $I = 3/2$ nuclear spin. The small-to-vanishing anisotropic component seen with CO dehydrogenase contrasts sharply with the large anisotropy in Cu(II) centers, where large *negative isotropic and negative anisotropic* $^{63,65}\text{Cu}$

couplings are typically observed: $a_{\text{iso}}(^{63,65}\text{Cu}) \sim T_{\text{max}}(^{63,65}\text{Cu}) \sim -[150-200] \text{ MHz}^{30-32}$; for a type 2 Cu(II) center, $a_{\text{iso}}(^{63,65}\text{Cu}) \sim T_{\text{max}}(^{63,65}\text{Cu}) \sim -70 \text{ MHz}$ for a type I Cu.^{33,34} No less startling, the ENDOR/PESTRE measurements show that the observed isotropic $^{63,65}\text{Cu}$ hyperfine coupling is positive, *opposite in sign* to those of d^9 Cu(II) centers with an unpaired electron in a ($d\sigma^*$) orbital. The Cu hyperfine couplings in CO dehydrogenase are instead consistent with a d^{10} Cu(I) ion whose closed-shell electronic configuration acquires a large *positive* a_{iso} through delocalization of the electron spin in the 'Mo(V) SOMO' over the entire [Mo(V)-(μ-S)-Cu(I)] unit, into the 4s orbital of Cu.

In support of this assignment, we observe that the Cu(I) hyperfine coupling seen here is quite similar to that of Cu(I) in an inorganic model compound prepared by Gourlay *et al.*,³⁵ which mimics the structure and spectroscopic properties of the paramagnetic active site of CO dehydrogenase: $[\text{Tp}^{\text{iPr}}\text{Mo}(\text{V})(\text{O})(\text{OAr})(\mu\text{-S})\text{Cu}(\text{I})(\text{Me}_3\text{tcn})]$ (where Tp^{iPr} = hydrotris(3-isopropylpyrazol-1-yl)borate; OAr = 3,5-(di-*t*-butyl)phenolate; Me_3tcn = 1,4,7-trimethyl-1,4,7-triazacyclononane). The isotropic Cu(I) hyperfine interaction, $|a_{\text{iso}}(^{63,65}\text{Cu})| \sim 159 \text{ MHz}$, observed for this model is quite similar in magnitude to $a_{\text{iso}}(^{63,65}\text{Cu}) = +148 \text{ MHz}$ seen with CO dehydrogenase. Calculations on the model have confirmed that the remarkably large values of a_{iso} reflect a strong covalent delocalization of the SOMO through the bridging sulfido.

The hyperfine coupling to ^{13}C in the EPR signal manifested by ^{13}CO -reduced CO dehydrogenase also is distinctive in being highly isotropic. The isotropic coupling, $a_{\text{iso}}(^{13}\text{C}) = +17.4 \text{ MHz}$, is intermediate between the values observed to date for carbon-containing ligands to a paramagnetic Mo(V) center: $a_{\text{iso}}(^{13}\text{C}) = +43.8 \text{ MHz}$ for formaldehyde-inhibited xanthine oxidase^{24,36,37,32} and $|a_{\text{iso}}(^{13}\text{C})| = 7.9 \text{ MHz}$ for the 'very rapid' Mo(V) intermediate trapped with that enzyme^{10,38}. Additionally, the anisotropic component seen here with CO dehydrogenase, $T = 0.73 \text{ MHz}^{39}$, is smaller than that observed in the formaldehyde-inhibited xanthine oxidase ($T = 3.8 \text{ MHz}$) and slightly smaller than that observed in the 'very rapid' intermediate ($T = 1.15 \text{ MHz}$). We therefore argue that this small isotropic ^{13}C coupling is unlikely to arise from a species with a Mo-C bond.

One possible assignment for the state studied here is Structure A of Fig 2. Our recent ^1H and ^{13}C -ENDOR study of the formaldehyde-inhibited Mo(V) of xanthine oxidase^{24,37,40} has shown that it possesses the core of four-membered ring structure D, with a Mo-C distance of 2.76 \AA in the DFT-optimized geometry.^{24,40} This structure resembles that of structure A' (Fig 2), found by X-ray diffraction of *n*-butylisonitrile-inhibited CO dehydrogenase (with a Mo-C distance of 2.63 \AA)⁶. The planar geometry of the related Structure D, with short Mo-C distance within the ring, favors strong covalent spin delocalization via the Mo-O-C linkage or a strong "transannular hyperfine interaction" between Mo(V) d_{xy} orbital and carbon 2s orbitals, resulting in an extremely large hyperfine coupling to the ^{13}C of formaldehyde, with $a_{\text{iso}} = 44.6 \text{ MHz}^{24}$. The significantly smaller hyperfine coupling for ^{13}C seen here with CO dehydrogenase thus argues against Structure A of Figure 2 being responsible for the observed EPR signal.

A second possible assignment of the Mo(V) species studied here is the five-membered metallocyclic ring of Structure B (Fig 2), the closest established analogue of which is the

species giving rise to the “glycol-inhibited” Mo(V) EPR signal of desulfo xanthine oxidase (Figure 2, Structure E). The ^1H -ENDOR results for the “glycol-inhibited” species were interpreted in terms of a five-membered (Mo-O-C-C-O) metallocyclic structure^{24,37}. The paramagnetic Mo(V) species giving rise to the “very rapid” EPR signal seen with xanthine oxidase also has a Mo-O-C unit analogous to that of Structure B. Here, the slow substrate 2-hydroxy-6-methylpurine⁹ is bound to the Mo(V) ion via the equatorial oxygen atom after being incorporated into product as a hydroxyl group^{10,41}. When the C-8 position of 2-hydroxy-6-methylpurine is labeled with ^{13}C , a_{iso} for the “very rapid” signal is 7.9 MHz²⁴, while a_{iso} for the ^{13}C of glycol in the glycol-inhibited signal is even smaller at 6.2 MHz (Shanmugam *et al.*, unpublished). In both cases, the ^{13}C hyperfine coupling is weak because there is no direct bonding of carbon to Mo(V) and the Mo-C distance is long (~ 3.4 Å), precluding strong overlap between Mo(V) d_{xy} and carbon 2s orbitals. The DFT results for structure B yield a very large a_{iso} for ^{13}C of 54 MHz, however, much larger than observed experimentally. The calculated copper hyperfine also is highly rhombic, $\mathbf{A}^{(63,65)\text{Cu}} = [19, -94, 105]$ MHz, in sharp disagreement with the observed isotropic coupling seen here with CO dehydrogenase. These observations argue against Structure B being responsible for the signal seen with CO dehydrogenase.

It is noteworthy that a recent X-ray crystallography study of the glycol- and glycerol-inhibited Mo centers of AOR claims a third structure variant, a direct Mo-C bond (structure F) for this species.¹⁹ However, if for illustrative purposes we assume that the dipolar interaction arises solely from a through-space interaction of the ^{13}C with a point electron spin on Mo(V), the measured value $T = 0.73$ MHz corresponds to a Mo-C distance of ~ 2.4 Å. Subtraction of a ^{13}C local contribution to the observed $T_{\text{obs}} = 0.73$ MHz, would further increase the resultant Mo-C distance¹⁰, thus ruling out a direct Mo-C bond in CO dehydrogenase. A similar analysis¹⁰ has helped rule out a direct Mo-C bond in the “very rapid” Mo(V) signal of xanthine oxidase prepared with 2-hydroxy-6-methylpurine (^{13}C -8).

Overall, a comparison of the ^{13}C coupling seen here (Table 2) with previously reported ^{13}C hyperfine tensors for a ligand to the paramagnetic Mo(V) enzyme species indicates that Structures A and B, as well as any structure with a Mo-CO bond, are unlikely to represent the structure of the binuclear center of CO dehydrogenase. Instead we propose that Structure C of Figure 2, with CO coordinated to the copper of the Mo(V)-Cu(I) binuclear center best represents the structure seen in the enzyme.

A structure having a Cu(I)-coordinated CO is consistent with both of the computational studies of the reaction of CO dehydrogenase that identify CO coordinated to the copper of a fully oxidized binuclear center as the starting point for catalysis^{12,13}. In the case of the partially reduced complex examined in the present study, with the molybdenum in the EPR-active Mo(V) valence state, the enzyme cannot progress through the catalytic sequence, thus accounting for the accumulation of the signal in the course of our sample preparation. Our Mo(V)/Cu(I)•CO species in fact represents a paramagnetic analog to the *bona fide* Michaelis complex for the reaction, and is thus analogous to the species giving rise to the well-characterized “Rapid” Mo(V) EPR signals in the related molybdenum-containing enzyme xanthine oxidase⁴² (albeit with a substantively different structure).

Although there is no EPR or ENDOR evidence regarding protonation of the equatorial Mo=O group in the Mo(V) state, our DFT calculations (Table 2) indicate that the observed *g*-tensor anisotropy is not consistent with a dioxo species such as seen in the oxidized enzyme^{6,7}. Coupled uptake of protons with electrons is a common property of even the simplest molybdenum complexes,^{43,44} and there is precedent for equatorial Mo-OH protons being only very weakly coupled.^{45,46} We thus consider it likely that the partially reduced binuclear center in fact possesses an equatorial Mo-OH (in contrast to the equatorial Mo=O of oxidized enzyme^{6,7}) in the Mo(V) state.

Conclusion

Our ENDOR results provide direct experimental support for CO coordination to Cu(I) of the binuclear center of CO dehydrogenase. Upon binding of CO, the reaction progresses as shown in Figure 7 by nucleophilic attack of the equatorial Mo=O oxygen on the Cu-bound CO, with substrate likely activated to at least some degree by backbonding from the copper which leads to population of the CO π^* orbital. The DFT calculations of Hofmann and coworkers¹³ indicate that this chemistry leads to a set of three species having the structures shown in brackets in Figure 7. Although presented as discrete intermediates in the computational work, we consider it likely that these species are readily interconverted. We further observe that they involve bonding of the carbon of substrate to each of the three atoms of the Mo- μ (S)-Cu core, and that subsequent work has shown each of the three core atoms to contribute significantly to the redox-active orbital³⁵. We therefore present these species in Figure 7 as an ensemble of states from which the reaction proceeds further. Completion of the catalytic sequence involves formal reduction of the binuclear cluster and formation of CO₂ from this ensemble, with hydroxide from solvent necessarily being introduced into the molybdenum coordination sphere to regenerate the equatorial ligand of the molybdenum and complete the catalytic cycle.

In summary, the ENDOR and computational study presented here provides direct experimental evidence that the EPR signal seen in the course of substrate reduction of CO dehydrogenase arises from a partially reduced, Mo(V)/Cu(I), binuclear center with CO bound at the copper. This conclusion provides strong support for a reaction mechanism that begins with a fully oxidized binuclear center, with CO coordinated to copper and thereby activated for nucleophilic attack by the equatorial Mo=O ligand.

Supplementary Material

Refer to Web version on PubMed Central for supplementary material.

Acknowledgments

The authors wish to acknowledge the support of the National Institutes of Health (GM 057378 to MLK), the National Science Foundation (MCB 0723330 to BMH, DGE-0824162 to GEC) and the Department of Energy (13ER16411 to RH).

ABBREVIATIONS

CO dehydrogenase	Carbon monoxide dehydrogenase
XO	Xanthine oxidase
AOR	aldehyde oxidoreductase

References

1. Meyer O, Lalucat J, Schlegel HG. *International Journal of Systematic Bacteriology*. 1980; 30:189.
2. Hille R. *Chemical Reviews*. 1996; 96:2757. [PubMed: 11848841]
3. Hille R. *Trends in Biochemical Sciences*. 2002; 27:360. [PubMed: 12114025]
4. Wilcoxon J, Zhang B, Hille R. *Biochemistry*. 2011; 50:1910. [PubMed: 21275368]
5. Dobbek H, Gremer L, Meyer O, Huber R. *Proceedings of the National Academy of Sciences of the United States of America*. 1999; 96:8884. [PubMed: 10430865]
6. Dobbek H, Gremer L, Kiefersauer R, Huber R, Meyer O. *Proceedings of the National Academy of Sciences of the United States of America*. 2002; 99:15971. [PubMed: 12475995]
7. Zhang B, Hemann CF, Hille R. *Journal of Biological Chemistry*. 2010; 285:12571. [PubMed: 20178978]
8. Wilcoxon J, Snider S, Hille R. *Journal of the American Chemical Society*. 2011; 133:12934. [PubMed: 21774528]
9. McWhirter RB, Hille R. *Journal of Biological Chemistry*. 1991; 266:23724. [PubMed: 1660883]
10. Manikandan P, Choi EY, Hille R, Hoffman BM. *Journal of the American Chemical Society*. 2001; 123:2658. [PubMed: 11456936]
11. Bray RC, Vanngard T. *Biochemical Journal*. 1969; 114:725. [PubMed: 4310055]
12. Siegbahn PEM, Shestakov AF. *Journal of Computational Chemistry*. 2005; 26:888. [PubMed: 15834924]
13. Hofmann M, Kassube JK, Graf T. *Journal of Biological Inorganic Chemistry*. 2005; 10:490. [PubMed: 15971074]
14. Resch M, Dobbek H, Meyer O. *Journal of Biological Inorganic Chemistry*. 2005; 10:518. [PubMed: 16091936]
15. Davoust CE, Doan PE, Hoffman BM. *Journal of Magnetic Resonance Series A*. 1996; 119:38.
16. Doan PE, Telsner J, Barney BM, Igarashi RY, Dean DR, Seefeldt LC, Hoffman BM. *Journal of the American Chemical Society*. 2011; 133:17329. [PubMed: 21980917]
17. Solomon EI, Baldwin MJ, Lowery MD. *Chemical Reviews*. 1992; 92:521.
18. Romao MJ, Archer M, Moura I, Moura JGG, Legall J, Engh R, Schneider M, Hof P, Huber R. *Science*. 1995; 270:1170. [PubMed: 7502041]
19. Santos-Silva T, Ferroni F, Thapper A, Marangon J, Gonzalez PJ, Rizzi AC, Moura I, Moura JGG, Romao MJ, Brondino CD. *Journal of the American Chemical Society*. 2009; 131:7990. [PubMed: 19459677]
20. Werst MM, Kennedy MC, Houseman ALP, Beinert H, Hoffman BM. *Biochemistry*. 1990; 29:10533. [PubMed: 2271662]
21. Werst MM, Kennedy MC, Beinert H, Hoffman BM. *Biochemistry*. 1990; 29:10526. [PubMed: 2176871]
22. Houseman ALP, Oh BH, Kennedy MC, Fan CL, Werst MM, Beinert H, Markley JL, Hoffman BM. *Biochemistry*. 1992; 31:2073. [PubMed: 1311203]
23. Walsby CJ, Hong W, Broderick WE, Cheek J, Ortillo D, Broderick JB, Hoffman BM. *Journal of the American Chemical Society*. 2002; 124:3143. [PubMed: 11902903]
24. Shanmugam M, Zhang B, McNaughton RL, Kinney RA, Hille R, Hoffman BM. *Journal of the American Chemical Society*. 2010; 132:14015. [PubMed: 20860357]

25. Hille, R. *Metals in Biology: Applications of High-Resolution EPR to Metalloenzymes*. Hanson, G.; Berliner, L., editors. Vol. 29. 2010. p. 91
26. Roberts JE, Brown TG, Hoffman BM, Peisach J. *J Am Chem Soc*. 1980; 102:826.
27. Hori H, Ikeda-Saito M, Yonetani T. *J Biol Chem*. 1981; 256:7849. [PubMed: 6267028]
28. Doan PE. *Journal of Magnetic Resonance*. 2011; 208:76. [PubMed: 21075026]
29. Kinney RA, Hettterscheid DGH, Hanna BS, Schrock RR, Hoffman BM. *Inorganic Chemistry*. 2010; 49:704. [PubMed: 20000748]
30. Holm RH, Kennepohl P, Solomon EI. *Chem Rev*. 1996; 96:2239. [PubMed: 11848828]
31. LaCroix LB, Shadle SE, Wang YN, Averill BA, Hedman B, Hodgson KO, Solomon EI. *Journal of the American Chemical Society*. 1996; 118:7755.
32. Penfield KW, Gay RR, Himmelwright RS, Eickman NC, Norris VA, Freeman HC, Solomon EI. *Journal of the American Chemical Society*. 1981; 103:4382.
33. Roberts JE, Cline JF, Lum V, Gray HB, Freeman H, Peisach J, Reinhammar B, Hoffman BM. *J Am Chem Soc*. 1984; 106:5324.
34. Chow C, Chang K, Willett RD. *J Chem Phys*. 1973; 59:2629.
35. Gourlay C, Nielsen DJ, White JM, Knottenbelt SZ, Kirk ML, Young CG. *Journal of the American Chemical Society*. 2006; 128:2164. [PubMed: 16478141]
36. Howes BD, Bennett B, Bray RC, Richards RL, Lowe DJ. *Journal of the American Chemical Society*. 1994; 116:11624.
37. Howes BD, Bray RC, Richards RL, Turner NA, Bennett B, Lowe DJ. *Biochemistry*. 1996; 35:1432. [PubMed: 8634273]
38. Howes BD, Bray RC, Richards RL, Turner NA, Bennett B, Lowe DJ. *Biochemistry*. 1996; 35:3874.
39. Manikandan P, Choi EY, Hille R, Hoffman BM. *J Am Chem Soc*. 2001; 123:2658. [PubMed: 11456936]
40. Sempombe J, Stein B, Kirk ML. *Inorganic Chemistry*. 2011; 50:10919. [PubMed: 21972782]
41. Pauff JM, Zhang JJ, Bell CE, Hille R. *Journal of Biological Chemistry*. 2008; 283:4818. [PubMed: 18063585]
42. Hille R, Kim JH, Hemann C. *Biochemistry*. 1993; 32:3973. [PubMed: 8385992]
43. Stiefel EI, Gardner JK. *Journal of the Less-Common Metals*. 1974; 36:521.
44. Stiefel EI. *Proceedings of the National Academy of Sciences of the United States of America*. 1973; 70:988. [PubMed: 4515630]
45. Klein EL, Astashkin AV, Raitsimring AM, Enemark JH. *Coordination Chemistry Reviews*. 2013; 257:110. [PubMed: 23440026]
46. Astashkin AV, Hood BL, Feng CJ, Hille R, Mendel RR, Raitsimring AM, Enemark JH. *Biochemistry*. 2005; 44:13274. [PubMed: 16201753]

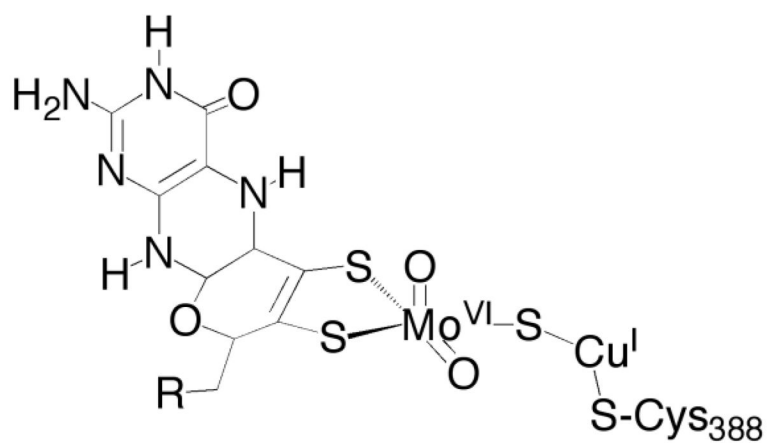


Figure 1. The active site of CO dehydrogenase from *O. carboxidovorans*. The molybdenum coordination geometry is approximately square-pyramidal, with the pyranopterin cofactor present as the dinucleotide of cytosine (R).

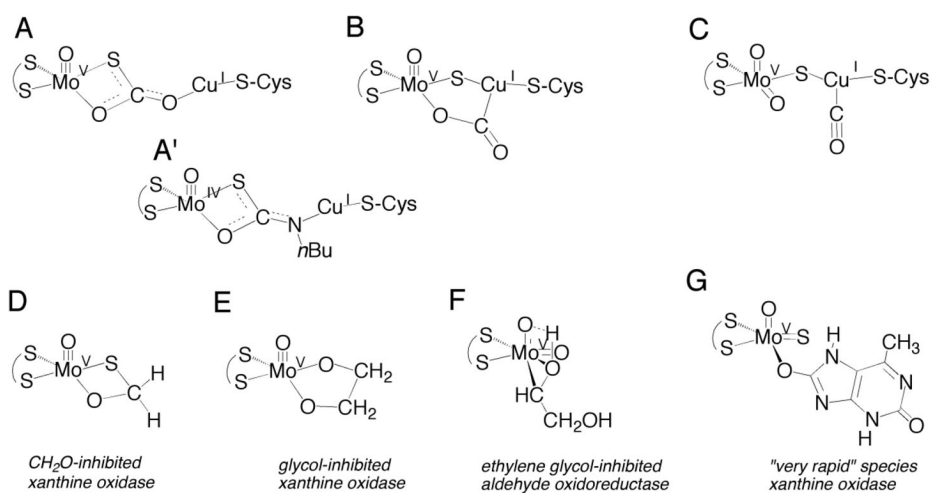


Figure 2. Possible structures for the EPR-active species seen with CO dehydrogenase (A–C), and structures of various relevant EPR-active Mo(V) species observed with the related enzyme xanthine oxidase (D–G).

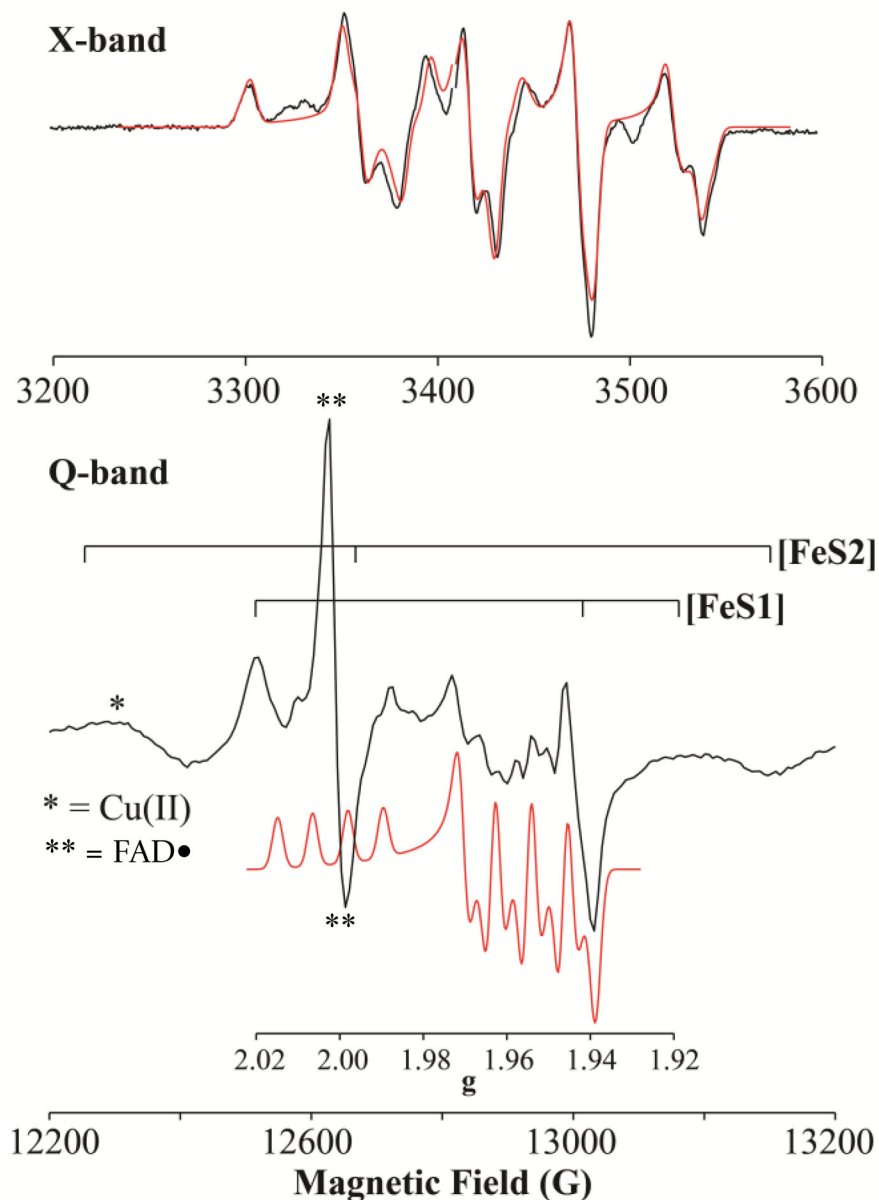


Figure 3. X-band (top) and Q-band (bottom) EPR spectra of the [Mo, Cu] center (black) in H₂O buffer at 150 K and 2 K respectively. (**Top**): 9.45 GHz, modulation amplitude = 5 G; red is the simulation with 150K parameters from Table 1. (**Bottom**): Numerical derivative of 34.8 GHz, two-pulse echo-detected spectrum (π -pulse = 80 ns, τ = 600 ns, repetition time = 50 ms). red: simulation of the binuclear signal using the 2K parameters from Table 1. g-scale included for correlation with ENDOR field-frequency patterns given in Figure 4. Note that the scale of this simulation is exaggerated relative to the intensity of the signal in the experimental spectrum to better illustrate line positions. The ‘braces’ show the field values for the canonical g-values of the FeS clusters. The asterisk denotes the signal of

adventitions Cu(II) in the signal, and the double asterisk the isotropic signal of FADH• from the enzyme, with $g = 2.00$.

Author Manuscript

Author Manuscript

Author Manuscript

Author Manuscript

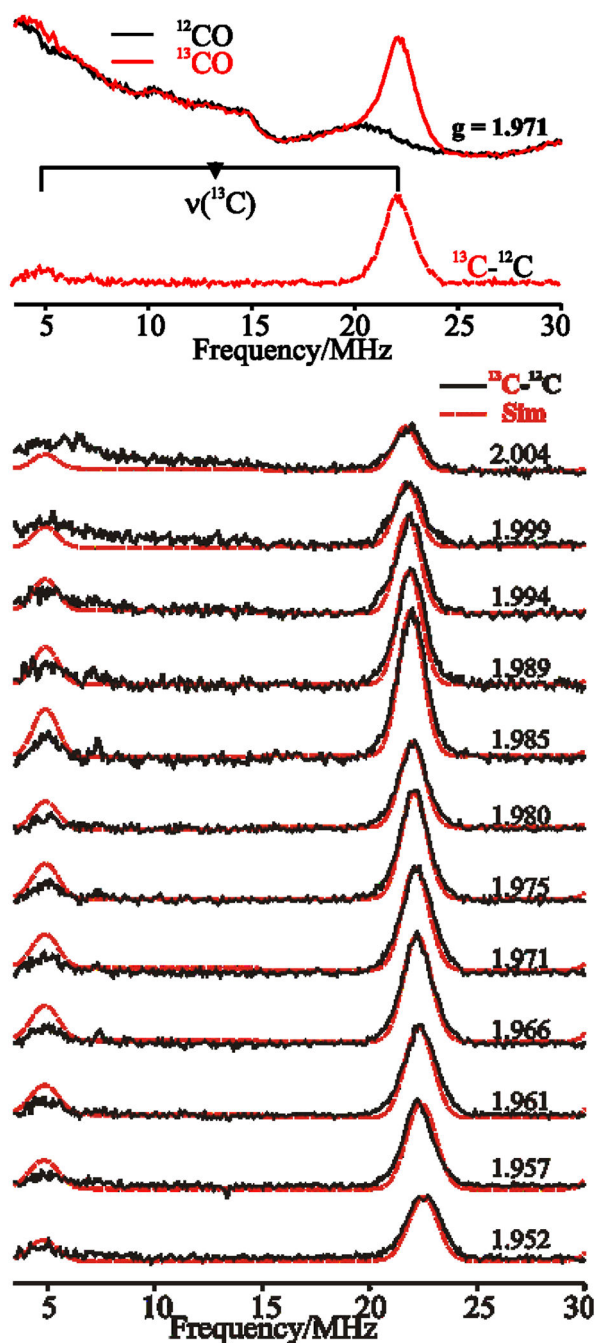


Figure 4.

Top, Davies ^{13}C -ENDOR spectra of the binuclear signal measured at $g = 1.971$. The red dotted line shows the ^{13}C hyperfine coupling, obtained by subtracting the spectrum of ^{12}CO (black line) from that of ^{13}CO (red line) in H_2O . The black horizontal bar connects the ^{13}C peaks centered at $\nu(^{13}\text{C})$ and separated by $A(^{13}\text{C})$. The low intensity of the low-frequency partner common in Q-band ENDOR. *Bottom*, simulated (red dotted lines) and experimental (black lines) 2-D field-frequency plot of Davies ^{13}C -ENDOR spectra of the binuclear signal reduced by ^{13}CO . The amplitudes of the simulated $\nu(^{13}\text{C})$ signals are multiplied by 1/3 to

reflect the low-intensities due to relaxation effects (see text). *Conditions:* π -pulse length = 120 ns, $\tau = 600$ ns, repetition time = 40 ms, microwave frequency = 34.795 GHz, $T = 2$ K.

Author Manuscript

Author Manuscript

Author Manuscript

Author Manuscript

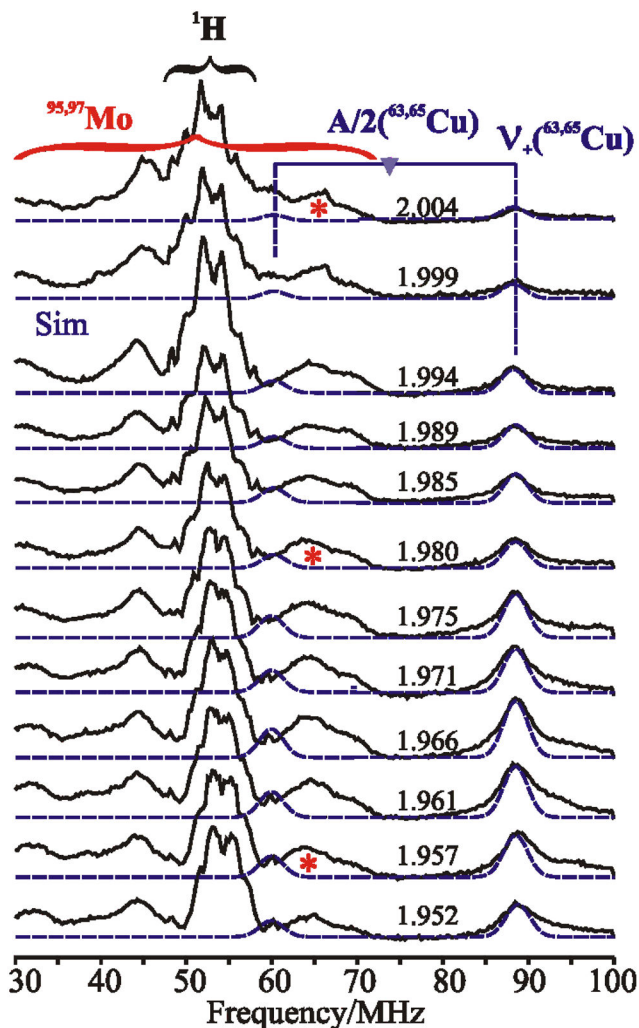


Figure 5.

2-D field-frequency plot of broad-band Davies ENDOR spectra of the binuclear signal reduced by ^{12}CO . The black brace encompasses the frequency range of ^1H signals; the red brace encompasses the frequency range of $^{95,97}\text{Mo}$ signals, with the (*) in representative spectra identifying resolved $^{95,97}\text{Mo}$ signals. Blue 'goalpost' connects the $^{63,65}\text{Cu}$ peaks at $\nu^+(^{63,65}\text{Cu}) \sim 87$ MHz and $\nu^-(^{63,65}\text{Cu}) \sim 60$ MHz; the center frequency is $A(^{63,65}\text{Cu})/2$ and separation is $2\nu(^{63,65}\text{Cu})$. Blue dotted lines are simulations of the $^{63,65}\text{Cu}$ spectra, where the amplitudes of the ν^- branches are multiplied by $1/2$ to reflect their low intensities.

Conditions: π -pulse length = 120 ns, τ = 600 ns, repetition time = 40 ms, microwave frequency = 34.772 GHz, T = 2 K.

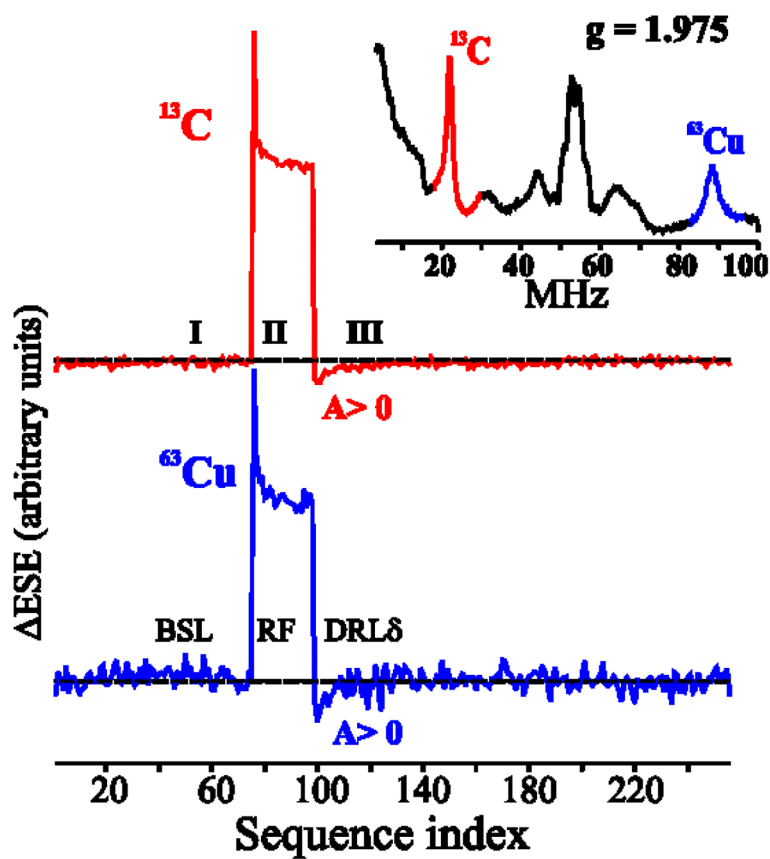


Figure 6. PESTRE spectra measured at the ν^+ peaks of the ^{13}C and $^{63,65}\text{Cu}$ nuclei (inset; indicated as red and blue lines) of the binuclear signal. The RF frequencies and the g value at which PESTRE experiments were carried out are given in the inset: *Conditions:* π -pulse length = 120 ns, $\tau = 600$ ns, repetition time = 40 ms, $t_{\text{RF}} = 20 \mu\text{s}$, microwave frequency = 34.795 GHz, $T = 2$ K.

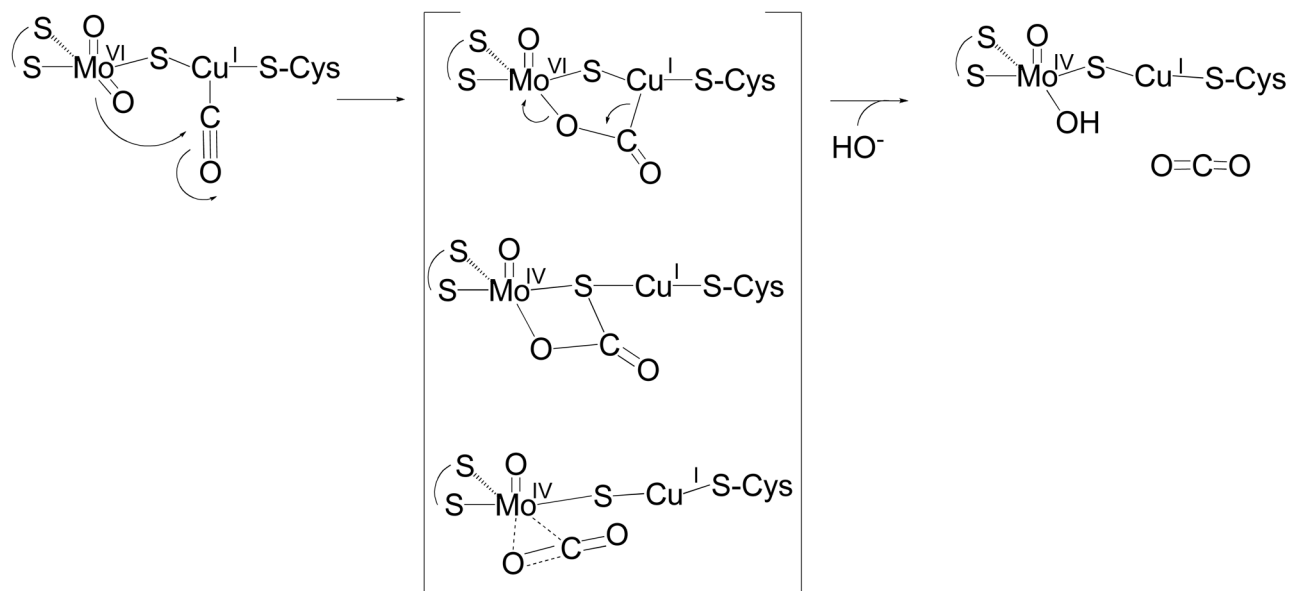
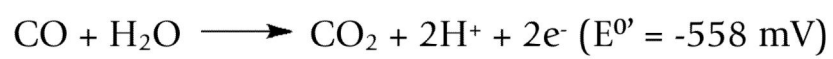


Figure 7.
The reaction mechanism of CO dehydrogenase.



Scheme 1.

Author Manuscript

Author Manuscript

Author Manuscript

Author Manuscript

Table 1

Spin Hamiltonian parameters used to simulate^a the 2-D ENDOR patterns of ¹³C and ^{63,65}Cu nuclei of Cu-CO dehydrogenase.

Nuclei	A_1	A_2	A_3	a_{iso}
¹³ C	+16.7	+16.5	+18.8	+17.33
^{63,65} Cu(ENDOR) ^b	+148	+148	+148	+148
^{63,65} Cu(EPR)	117	164	132	+137.6

^a Simulations employed $\mathbf{g} = [2.002, 1.958, 1.953]$ and the hyperfine couplings are in MHz.

^b Quadrupole splitting for ^{63,65}Cu ($I = 3/2$) are not observed, their inclusion had no effect on simulations, so were not incorporated.

Table 2

Experimental and computed EPR parameters for CO-reduced CO dehydrogenase.^a

	g_{\min}	g_{mid}	g_{\max}	$^{63,65}\text{Cu } a_{\text{iso}}$	$^{63,65}\text{Cu } T$	$^{13}\text{C } a_{\text{iso}}$	$^{13}\text{C } T$	$^1\text{H } a_{\text{iso}}$	$^1\text{H } T$	$^{95,97}\text{Mo } a_{\text{iso}}$
Experiment	1.953	1.958	2.002	+148 ^b 138 ^c	-0 ^b [-20.7, +26.4, -5.7] ^c	17.3 ^b	[-6, -8, 1.5] ^b	N/A	N/A	75-100
MoO ₂ + CO bound to Cu(I)	1.911	1.950	1.996	167	-13, 2, 11	3.7	-4.5, -5.1, 9.7	N/A	N/A	59
Mo(O)(HCO ₃ ⁻)	1.949	1.967	2.022	281	-17, -7, 24	18.6	-1.0, -1.0, 2.0	3	-1, -1, 2	65
Mo(O)(OH)(CO)	1.954	1.958	2.015	90	-13, -8, 21	15.8	-2.6, -1.7, 4.4	4	-5, -7, 11	65
Mo(O)(OH) + CO bound to Cu(I) (constrained S-Cu-S at 139°)	1.955	1.959	2.012	137	-15, -7, 21	26.6	-3.5, -1.9, 5.5	4	-5, -7, 11	65

^a All hyperfine coupling constants are in MHz.

^b These values derive from the present 2K ENDOR measurements,

^c from the 150K X-band EPR spectrum (ref. 7).